Cell Reports
Physical Science

CellPress
OPEN ACCESS

Article

Realized potential as neutral pH flow batteries achieve high power densities

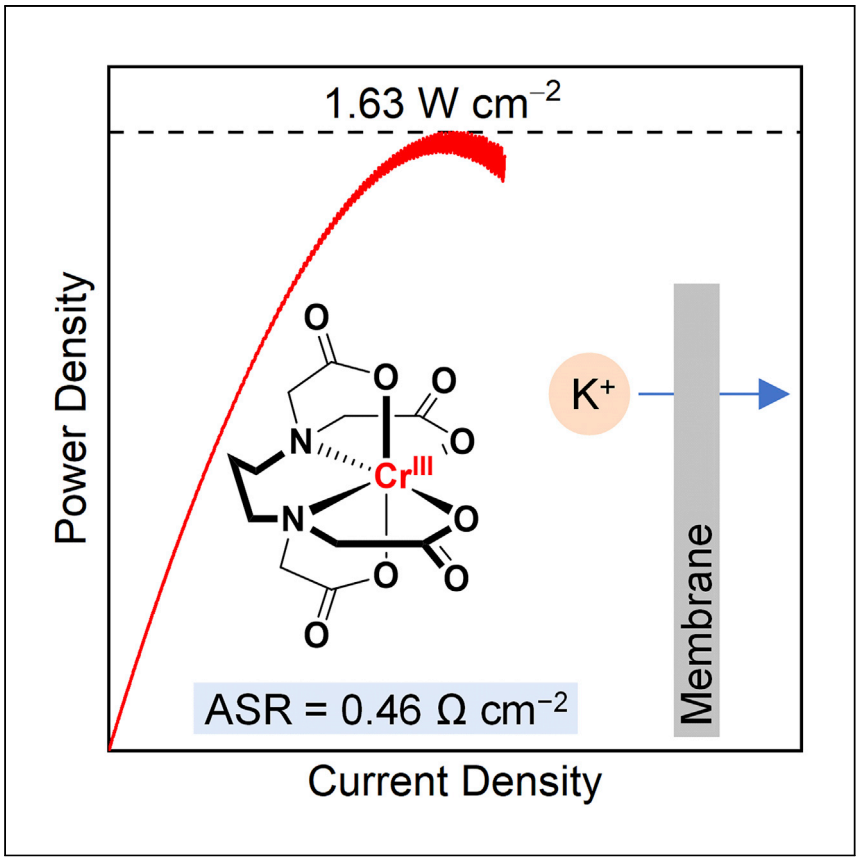

High-power flow battery operation lowers system costs but has previously required proton transport. By combining high voltage with low resistance from a highly selective and conductive membrane, Robb et al. demonstrate an aqueous flow battery that achieves record non-acidic power performance while utilizing potassium membrane transport at neutral pH.

Brian H. Robb, Scott E. Waters, James D. Saraidaridis, Michael P. Marshak

michael.marshak@colorado.edu

Highlights

High-power flow battery operates at neutral pH with potassium membrane transport

Record discharge-power performance for a flow battery not using proton transport

Inexpensive membrane provides high conductivity and constant efficiency cycling

Chelated metal electrolyte enables high voltage battery and high-power operation

Robb et al., Cell Reports Physical Science 3, 101118
November 16, 2022
https://doi.org/10.1016/j.xcrp.2022.101118

Cell Reports
Physical Science

CellPress
OPEN ACCESS

Article

Realized potential as neutral pH flow batteries achieve high power densities

Brian H. Robb,[2] Scott E. Waters,[1] James D. Saraidaridis,[3] and Michael P. Marshak[1,4,5,6,*]

SUMMARY

High power density operation of redox flow batteries (RFBs) is essential for lowering system costs, but until now, only acid-based chemistries have achieved such performance, primarily due to rapid membrane proton (H^+) transport. Here, we report a neutral pH RFB using the highly reducing Cr-(1,3-propylenediaminetetraacetate) (CrPDTA) complex that achieves acid-like power performance while utilizing potassium ion (K^+) transport. We investigate RFB resistance components and demonstrate the high and consistent K^+ conductivity of the Fumasep E-620(K) membrane. When combined with a robust bismuth electrocatalyst, this membrane enables constant voltage efficiency operation of a CrPDTA|$Fe(CN)_6$ RFB for 200 cycles. An optimized CrPDTA|$Fe(CN)_6$ RFB, which combines a high cell potential with a low area-specific resistance (0.46 Ω cm^2), demonstrates a maximum discharge power density of 1.63 W cm^{-2} and an average discharge power density over 500 mW cm^{-2} while maintaining 80% round-trip energy efficiency cycling, which are records for non-acid-based RFBs.

INTRODUCTION

Redox flow batteries (RFBs) are a promising long-duration (10+ h) energy storage (LDES) method, and many RFBs, including iron/chromium (FeCr RFBs) and vanadium (VRFBs), employ metal cations dissolved in corrosive acid as electroactive species.[1–5] FeCr RFBs, first investigated in the 1970s, utilize low-cost and abundant electrolyte species but suffer from performance and lifetime issues.[6–8] VRFBs, first demonstrated in 1986, offer a 1.4 V potential that can operate at high current densities but suffer from the volatile and sometimes high cost of vanadium, which can make VRFBs prohibitively expensive for LDES applications.[9,10] However, VRFBs have recently been successfully commercialized for moderate-duration (4–10 h) applications, in part due to the decreased VRFB stack costs enabled by the drastic performance gains in power density achieved through decades-long systematic optimization efforts in industry, academia, and national labs.[11–13] Despite the low cost of the FeCr RFB electrolytes, the low power density of the FeCr RFB results in higher power generation component costs and can cause the overall FeCr RFB cost to be more expensive than VRFBs.[7] For LDES RFBs, combining low-cost electrolytes and high power density operation can achieve exceptionally low overall system cost. Much work has rightly focused on lowering energy costs through novel electrolytes, but many cannot achieve the same power as the VRFB, or even the FeCr RFB, making the power costs an important contributor to overall system costs.[14]

RFBs use a membrane or separator to prevent mixing between the negative electrolyte (anolyte) and positive electrolyte (catholyte). The membrane should allow ionic transport to maintain charge balance while preventing electroactive species

[1]Department of Chemistry, University of Colorado Boulder, Boulder, CO 80309, USA

[2]Department of Chemical and Biological Engineering, University of Colorado Boulder, Boulder, CO 80309, USA

[3]Raytheon Technologies Research Center, East Hartford, CT 06108, USA

[4]Renewable and Sustainable Energy Institute, University of Colorado Boulder, Boulder, CO 80309, USA

[5]Twitter: @michaelmarshak

[6]Lead contact

*Correspondence: michael.marshak@colorado.edu

https://doi.org/10.1016/j.xcrp.2022.101118

crossover to maximize coulombic efficiency (CE) and minimize capacity loss. Acid-based RFBs can adapt cation-exchange membranes (CEMs) optimized for rapid proton (H^+) transport in fuel cells, resulting in RFBs with high membrane conductivity and low ohmic resistance (R_Ω). However, common CEMs, such as Nafion 212, generally provide lower conductivity for cations other than H^+, such as potassium (K^+), causing non-acid-based RFBs to have higher R_Ω values.[15] The total resistance of an RFB is composed of the R_Ω, charge transfer resistance (R_{ct}) and mass transport resistance (R_{mt}) and is normalized by area to give a full cell area-specific resistance (ASR). Improvements to ASR can be achieved through resistance-lowering techniques such as increasing membrane conductivity (R_Ω), using an electrocatalyst (R_{ct}), and decreasing solution viscosity (R_{mt}). For aqueous RFBs to be economically viable, a maximum plausible ASR of approximately 1.5 Ω-cm^2 has been calculated for RFBs below 1.5 V.[16,17] Electrochemical impedance spectroscopy (EIS) with 1 M KCl solutions has shown that RFBs assembled with H_2O-soaked and 1 M KCl-soaked Nafion 212 membranes exhibit initial R_Ω values of 0.8 and 2.7 Ω-cm^2, respectively, with the H_2O-soaked R_Ω increasing over time.[15] While CEMs were often intentionally optimized around H^+ transport for fuel cell or acid-based RFB applications, many recent flow battery chemistries, such as electroactive organic or metal-organic molecules, operate in neutral/alkaline conditions and therefore require non-H^+ ion transport.[14] The chemistries based on K^+ ion transport would benefit from similar membrane design optimizations for rapid and constant K^+ conductivity, as the R_Ω for these RFBs is normally the largest portion of their ASR.[18,19]

In principle, RFBs can operate at any round-trip energy efficiency (EE) by altering operating parameters such as power or current density. However, typically 80% EE is targeted in commercial systems because it balances power output and efficiency losses for optimal cost of energy storage at present electricity prices.[3,7] The RFBs that have demonstrated the highest discharge power densities at 80% round-trip EE all conduct H^+ but have required long-term systematic optimization to achieve this performance (Figure 1).[10–13,18,20–33] The expected average discharge power density that an RFB can provide while achieving 80% EE cycling can be approximated from Equation 1 (see supplemental information, expected discharge power density, for derivation):

$$P_{80} = \frac{0.09 \times V_{cell}^2}{R}, \qquad \text{(Equation 1)}$$

where P_{80} is the average discharge power density in W cm^{-2}, V_{cell} is the RFB open circuit potential (OCP) in V at 50% state of charge (SOC), and R is the ASR of the cell in Ω cm^2. Since discharge power density scales with V^2/R, higher voltage RFBs have a unique advantage to achieving high discharge power densities without requiring an H^+-level ASR, thus enabling the possibility of high-power K^+ operation. Furthermore, when water-splitting reactions are minimized through kinetic stabilization, high-voltage aqueous RFBs above 1.5 V are possible and can provide a significant reduction in capital costs associated with both system energy and power.[34,35]

We have previously reported a promising aqueous RFB anolyte electroactive species that operates at near-neutral pH and utilizes a chelating agent, 1,3-propylenediaminetetraacetic acid (PDTA), bound to chromium to create a robust Cr-chelate complex (CrPDTA).[20,36] The potassium salt of the $CrPDTA^-$ anion (KCrPDTA) exhibits high solubility (1.32 M) and a very negative reduction potential (−1.10 V versus SHE).[20,37] RFBs utilizing KCrPDTA paired with a ferro/ferricyanide catholyte ($Fe(CN)_6^{4-/3-}$) and operated near pH 9 with a boric acid ($B(OH)_3$)/potassium tetraborate ($K_2B_4O_7$) buffer and a Nafion 212 CEM have demonstrated a high cell potential

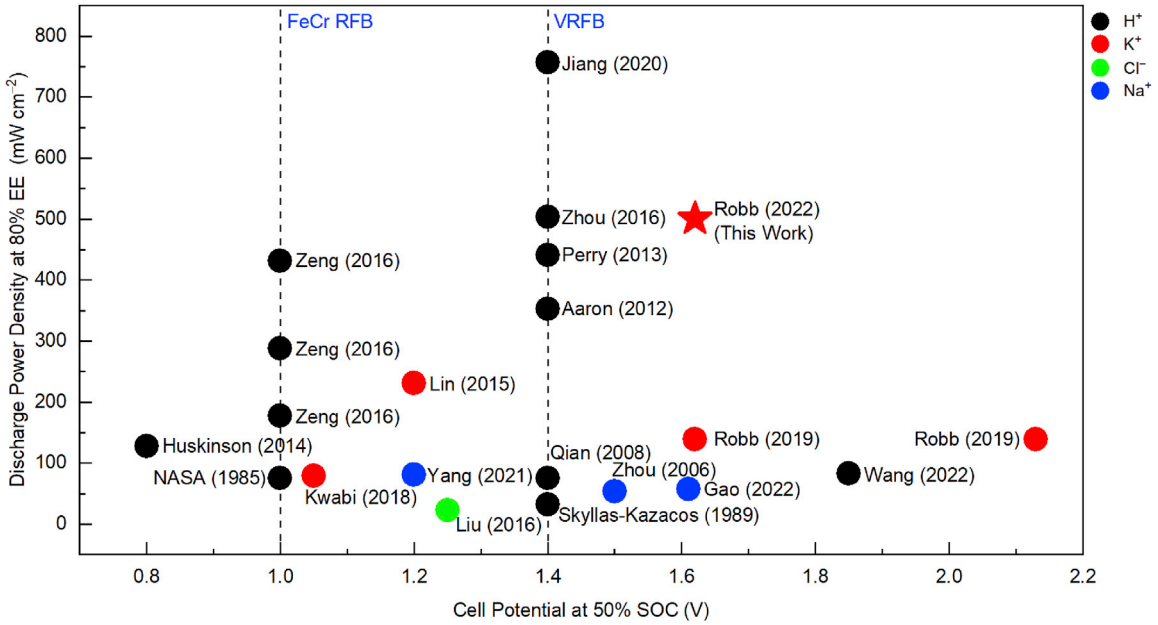

Figure 1. High-performance RFB discharge power density comparison

A comparison of the average discharge power density at 80% EE cycling and equilibrium cell potential (OCP at 50% SOC) for select high-performance RFBs. Color denotes charge carrier ion.

(1.62 V) and high CE (>99.5%).[15,19,20,38] The reduced Cr(II)PDTA^{2-} has been shown to exhibit long-term stability and a low self-discharge rate (<0.1% per day), leaving small CE losses in the system to be attributed to trace O_2 permeation or trace H_2 generation at the electrode from metal impurities catalyzing the hydrogen evolution reaction (HER).[36,39] The byproduct of these CE losses results in an increase in solution pH, requiring a buffer to maintain the pH below 11, the upper stability range of CrPDTA.[20] Compared with FeCr RFBs, the larger sizes and negative charges of CrPDTA and $Fe(CN)_6$ result in minimal crossover through Nafion 212.[7,15,20,40] However, for long-term RFB cycling, a membrane that eliminates crossover of these two species is desired. Similarly, for long-term RFB viability, constant voltage efficiency (VE) performance is desired, and RFBs using 1 M CrPDTA and Nafion 212 have exhibited a slow downward trend in VE during cycling, leading us to investigate and rectify the cause of the ASR change over time.[15,19,38,41]

The Fumasep E-620(K) membrane has demonstrated high K^+ conductivity within RFBs and has exhibited undetectable CrPDTA crossover rates due to channel size-based exclusion.[18,42–45] Fumasep E-600(K) series membranes (E-600(K) membranes) are available in different thicknesses (e.g., E-620(K) is 20 μm), are non-fluorinated, and are composed of a sulfonated polyaryletherketone-copolymer backbone.[18] Nafion membranes are fluorinated and based on a perfluorosulfonic acid (PFSA) polymer.[3] A fluorinated membrane that is resistant to oxidation is required for some highly oxidizing RFB electrolytes, such as $V^{4+/5+}$ (0.99 V versus SHE) but not for reducing species like CrPDTA nor mildly oxidizing species like $Fe(CN)_6^{4-/3-}$ (0.36 V versus SHE).[46,47] However, PFSA membranes are expensive ($500–$700 m^{-2}) and can account for a substantial portion of overall RFB system costs.[7,48] The low permeability and inexpensive, non-fluorinated nature of E-600(K) membranes suggests that they could be low cost (in $/kW) and could enable long-lasting CrPDTA|$Fe(CN)_6$ RFBs. Here, we systematically probe specific aspects of the RFB system and their effect on both short-term cell ASR

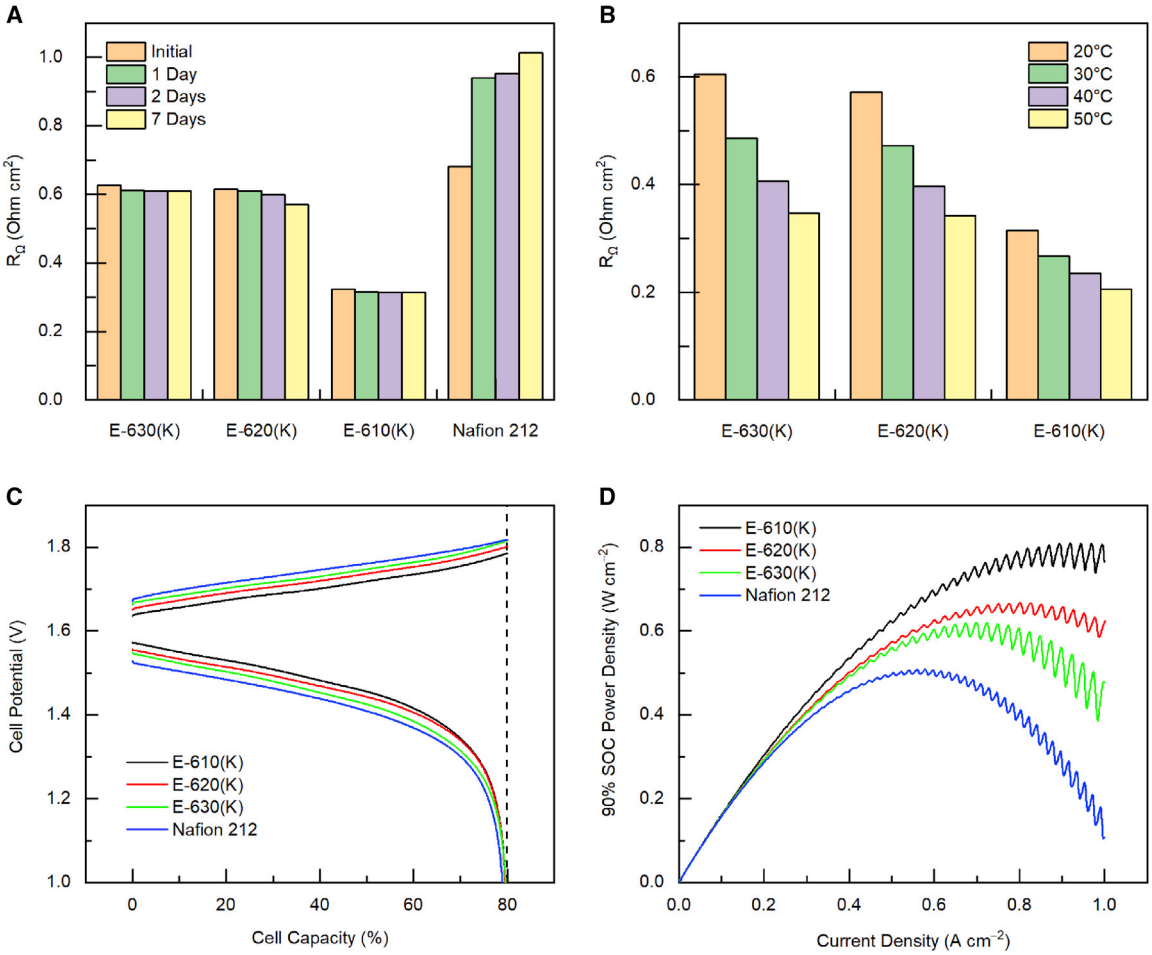

Figure 2. Cell resistance and performance data comparison for select membranes

(A) Time-based R_Ω of RFBs with 1 M KCl solution. See also Figure S2.

(B) Temperature-based R_Ω of RFBs with 1 M KCl solution. See also Figure S3.

(C) Cell potential as a function of capacity for a single cycle at $\pm$100 mA cm^{-2} of 1.0 M CrPDTA in 0.2 M $B(OH)_3$/0.05 M $K_2B_4O_7$ versus 0.5 M $K_4Fe(CN)_6$/0.1 M $K_3Fe(CN)_6$ with 0.025 M $K_2B_4O_7$.

(D) Discharge power density as a function of current density at 90% SOC for solutions from (C). See also Figure S10.

and long-term VE consistency using Fumasep E-600(K) and Nafion membranes. The ability to tailor cell components to systematic needs is then exemplified in a high power and current density, K^+-based CrPDTA|$Fe(CN)_6$ RFB, which achieves constant VE operation.

RESULTS AND DISCUSSION

Initial membrane investigation

To determine the long-term viability of E-600(K) membranes for CrPDTA|$Fe(CN)_6$ RFBs, the membrane K^+ conductivity performance was investigated. The R_Ω of cells built with Nafion 212 and E-600(K) membranes was measured over time via EIS with 1 M KCl solutions (see supplemental information, electrochemical impedance spectroscopy). The initial R_Ω values for all E-600(K) membranes were lower than that of Nafion 212, and over 7 days, the R_Ω for all E-600(K) membranes slightly decreased while that of Nafion 212 increased (Figures 2A, S1, and S2). This constant or improved R_Ω over time makes the E-600(K) membranes ideal candidates to enable constant VE performance for chemistries utilizing K^+ transport. Elevated

Table 1. Cell resistance values, efficiency values at ±100 mA cm^{-2}, and peak discharge power density at 90% SOC for E-600(K) or Nafion 212 separated RFBs with KCl solutions or CrPDTA versus Fe(CN)$_6$ with borate buffer

Membrane	Initial 1 M KCl R_Ω (Ω cm^2)[a]	Initial ASR (Ω cm^2)	Average CE (%)	Average VE (%)	Peak discharge power density (mW cm^{-2})
E-610(K)	0.31 ± 0.01	0.86 ± 0.02	99.9 ± 0.1	85.0 ± 0.5	810
E-620(K)	0.53 ± 0.03	1.15 ± 0.05	99.9 ± 0.1	84.1 ± 0.3	668
E-630(K)	0.55 ± 0.01	1.20 ± 0.03	99.9 ± 0.1	82.8 ± 0.4	620
Nafion 212	N/A	1.41	99.7	80.8	508

[a]A shorted (membraneless) RFB demonstrated an R_Ω of 0.1 Ω cm^2.[15]

temperatures are realized in large-scale RFB stacks when operating, so the R_Ω temperature dependence of the cells built with E-600(K) membranes was measured and showed a decreasing R_Ω from 20°C to 50°C (Figures 2B and S3).[49] These promising results justified full cell testing of E-600(K) membranes in CrPDTA|Fe(CN)$_6$ RFBs.

Full cell CrPDTA|Fe(CN)$_6$ RFB experiments were then performed with anolytes (pH 8.5) with either PDTA or borate buffer and catholytes with an 25% excess of Fe(II) (Table S1). An excess of catholyte is used to ensure that the anolyte remains the capacity-limiting side, as trace CE losses slowly shift the SOC of the catholyte. Triplicate RFBs were constructed with a single H_2O-soaked E-610(K), E-620(K), or E-630(K) membrane, and EIS with 1 M KCl was performed to determine average initial R_Ω for each cell (Table 1; Figures S4). An anolyte consisting of 1.0 M KCrPDTA with 0.2 M $B(OH)_3$/0.05 M $K_2B_4O_7$ (pH 8.5; 10 mL) and a catholyte consisting of 0.5 M $K_4Fe(CN)_6$/0.1 M $K_3Fe(CN)_6$ with 0.025 M $K_2B_4O_7$ (pH 9.2; 25 mL) were added, and an initial linear current sweep was performed at 500 mA s^{-1} to obtain an ASR, followed by three cycles each at ±50, 75, 100, 125, and 150 mA cm^{-2} to 80% CrPDTA capacity (Table 1; Figures S5–S7). The full cell cycling was repeated with a single Nafion 212 RFB, which provided results consistent with previous Nafion 212 cells (Table 1; Figures S8).[19,38] To investigate power performance, a single RFB was assembled with each membrane, and linear current sweeps at 500 mA s^{-1} were performed at 10, 25, 50, 75, and 90% SOC to generate polarization and power curves (Table 1; Figures S9 and S10). All E-600(K) membrane RFBs demonstrated lower ASRs and increased performance compared with Nafion 212 RFBs, with 2.8%, 4.4%, and 5.5% increases in VE at ±100 mA cm^{-2} and 22%, 31%, and 59% increases in peak power density at 90% SOC for E-630(K), E-620(K), and E-610(K), respectively (Figure 2C and 2D).

Extended E-620(K) cell cycling

To investigate if the R_Ω value of E-620(K) RFBs remained constant during CrPDTA|Fe(CN)$_6$ RFB cycling and if they could enable stable VE operation, extended cycling with E-620(K) RFBs was performed, with the remaining experiments utilizing a PDTA-buffered anolyte and an unbuffered catholyte. An E-620(K) RFB was assembled and cycled 100 times at ±100 mA cm^{-2} (Figures 3A and S11A; Table 2). Full cell EIS pre- and post-cycling confirmed that the R_Ω slightly decreases over the course of cycling, indicating that the K^+ conductivity of E-620(K) is not impacted by the highly reducing CrPDTA (Figures S11B). However, there is a small increase in the R_{ct}, which is observed in the slow decrease in VE during the 100 cycles.

Resistive heating within large-scale RFBs can result in operating temperatures reaching at least 40°C, which can decrease several RFB resistances, including improving electron transfer.[49] To investigate if elevated temperature operation could help

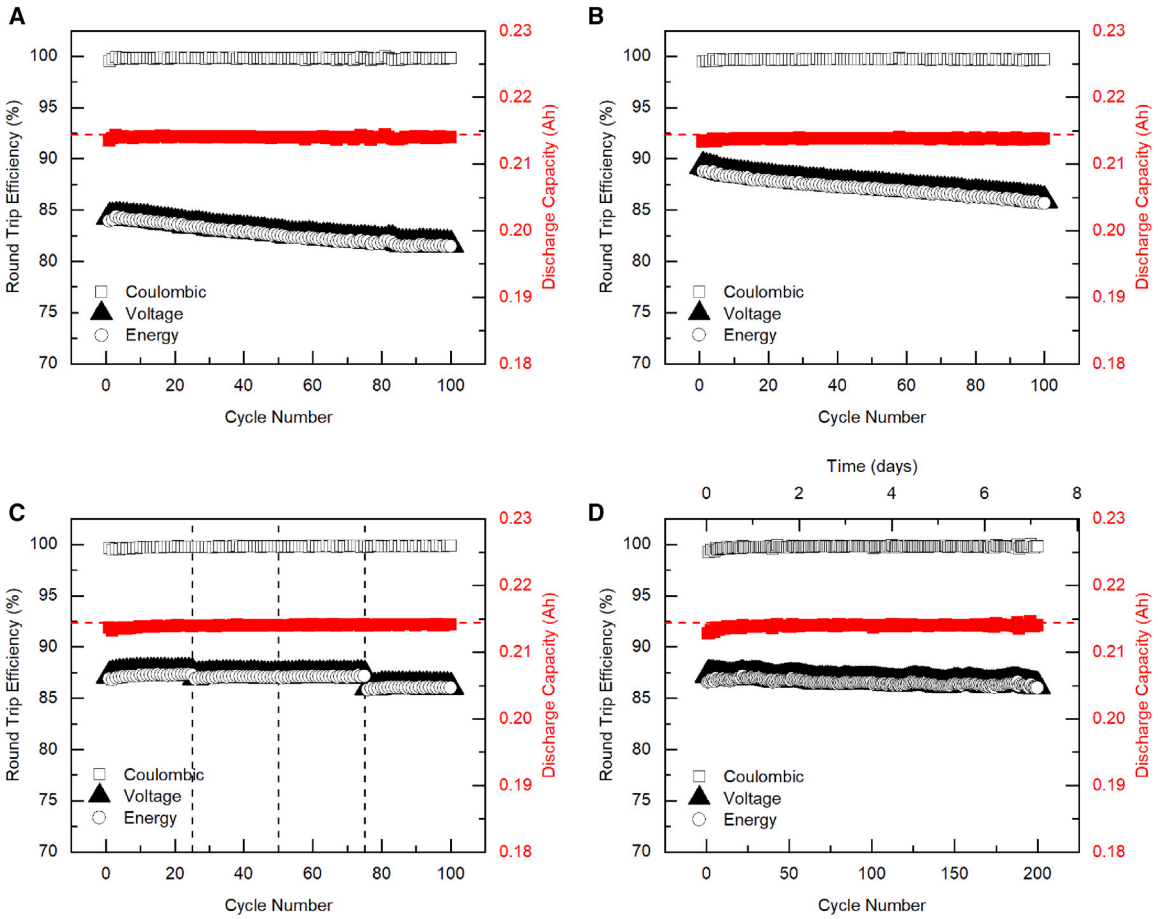

Figure 3. Extended cycling and high performance E-620(K) cell cycling data

(A) Discharge capacity and coulombic, voltage, and energy efficiency per cycle at $\pm$100 mA cm^{-2} for standard RFB setup with 1.0 M CrPDTA in 0.1 M PDTA versus unbuffered 0.5 M $K_4Fe(CN)_6$/0.1 M $K_3Fe(CN)_6$. Horizontal dashed line (red) represents 80% CrPDTA discharge capacity.

(B) Discharge capacity and cell efficiencies per cycle for 40°C cell at $\pm$100 mA cm^{-2} using same electrolyte setup as (A). Horizontal dashed line (red) represents 80% CrPDTA discharge capacity.

(C) Discharge capacity and cell efficiencies per cycle for Bi-Plated cell 1 at $\pm$100 mA cm^{-2} using same electrolyte setup as (A). Vertical dashed lines (black) indicate that EIS was performed. Horizontal dashed line (red) represents 80% CrPDTA discharge capacity.

(D) Discharge capacity and cell efficiencies per cycle for Bi-Plated cell 2 at $\pm$100 mA cm^{-2} using same electrolyte setup as (A). Horizontal dashed line (red) represents 80% CrPDTA discharge capacity.

could lead to constant VE CrPDTA|$Fe(CN)_6$ RFB cycling, we simulated realistic RFB conditions by operating an E-620(K) RFB at 40°C (E-620(K) maximum recommended operating temperature). The cell was cycled 100 times at $\pm$100 mA cm^{-2} to 80% CrPDTA capacity (Figures 3B and S12). The decreased resistances at 40°C associated with lower electrolyte viscosity (R_{mt}), improved membrane K^+ conductivity (R_Ω), and easier electron transfer (R_{ct}) resulted in a lowered ASR of 0.86 Ω cm^2 and no change to average CE, indicating no increase in HER. (Tables 2 and S2). However, a slow VE decrease was still observed, suggesting that elevated temperature is not able to prevent the slight R_{ct} increase.

We have previously demonstrated short-term RFB cycling with a bismuth electrocatalyst, which decreased R_{ct} by enabling reversible CrPDTA electron transfer kinetics.[19] The near-neutral pH and highly negative reduction potential of the CrPDTA anolyte should also enable long-term bismuth stability when cycling, especially compared with the anolytes of VRFBs and FeCr RFBs, which are less reducing

Table 2. Cell resistance and efficiency values for E-620(K) RFBs with 0.1 M PDTA buffered CrPDTA versus unbuffered $Fe(CN)_6$ operated at $\pm$100 mA cm^{-2}

RFB operating conditions (number of cycles)	Initial ASR (Ω cm^2)	Average CE (%)	Average VE (%)
Standard setup	1.22	99.8 $\pm$ 0.1	82.8 $\pm$ 0.9
Heated at 40°C (100)	0.86	99.7 $\pm$ 0.1	87.4 $\pm$ 0.8
Bi-plated cell 1 (1^{st} 25)	0.96	99.7 $\pm$ 0.1	87.5 $\pm$ 0.1
Bi-plated cell 2 (200)	0.99	99.8 $\pm$ 0.1	86.7 $\pm$ 0.3

and operate at bismuth-dissolving acidic conditions. Here, we investigated the application of the previously reported bismuth electrocatalyst on long-term R_{ct} and VE stability. The anodes of an E-620(K) RFB were plated with bismuth, following literature methods (0.58 mg cm^{-2} $electrode^{-1}$) (Bi-Plated Cell 1), and 100 cycles were performed at $\pm$100 mA cm^{-2} in 25 cycle increments.[19] A consistent VE was observed over each set of 25 cycles, with shifts in VE occurring between each set of cycles when the RFB was fully discharged and moved to perform EIS (Figures 3C and S13; Table 2 and S2). This indicates that the R_{ct} consistency from the anode bismuth electrocatalyst is key for achieving constant VE cycling with the CrPDTA|$Fe(CN)_6$ RFB.

To investigate long-term bismuth electrocatalyst performance, an identical Bi-plated E-620(K) RFB was assembled (Bi-Plated Cell 2) and cycled 200 times at $\pm$100 mA cm^{-2}, the highest number of cycles for a CrPDTA RFB, with an average VE of 86.7% (Figures 3D and S13C; Table 2). Following 200 cycles, EIS demonstrates that the R_{ct} improvement from the bismuth electrocatalyst remains unchanged after over a week of cycling, indicating that the highly reducing CrPDTA and non-acidic pH enable bismuth to remain stable on the electrode (Figure S13D).

During these 200 cycles, the anolyte solution pH increased from 8.5 to 10.5 due to trace HER generating OH^- over time. For longer cycling to further demonstrate CrPDTA|$Fe(CN)_6$ RFB stability, a method to reintroduce electrons lost to HER is required, such as the separate electrolyzer cell used with the FeCr RFB, to both maintain SOC balance between the anolyte and catholyte and to mitigate the slow anolyte pH increase and keep the CrPDTA electrolyte within its stable pH range.[7,22] Extended-duration cycling demonstrations using this technique is an area of study within the group.

Optimized E-610(K) cell cycling

We individually demonstrated the constant K^+ conductivity of E-600(K) membranes (R_Ω), the constant R_{ct} of CrPDTA|$Fe(CN)_6$ RFBs with a bismuth electrocatalyst, and the ability to lower the overall ASR of a CrPDTA|$Fe(CN)_6$ RFB through 40°C operation, a Bi-electrocatalyst, and an E-610(K) membrane. To realize the lowest ASR and highest performance CrPDTA|$Fe(CN)_6$ RFB while achieving constant VE, we combined these improvements, and an RFB was assembled that utilized E-610(K), Bi-plated anolyte electrodes, cell heating to 40°C, and the previously described electrolytes (optimized cell 1). The RFB was operated for 100 cycles at $\pm$200 mA cm^{-2} with constant VE and exhibited an average CE of 99.8%, an average VE of 88.0% and an initial and final ASR of 0.463 and 0.466 Ω cm^2, respectively (Figures 4A and S14). The majority of the low ASR value is a result of the R_Ω (0.234 Ω cm^2 from Figure 2B), so further tailored improvements for membrane K^+ conductivity would be most impactful for enabling even higher performance.

To investigate if consistent VE performance can be achieved at even higher current and power densities, an identical RFB (optimized cell 2) was assembled and

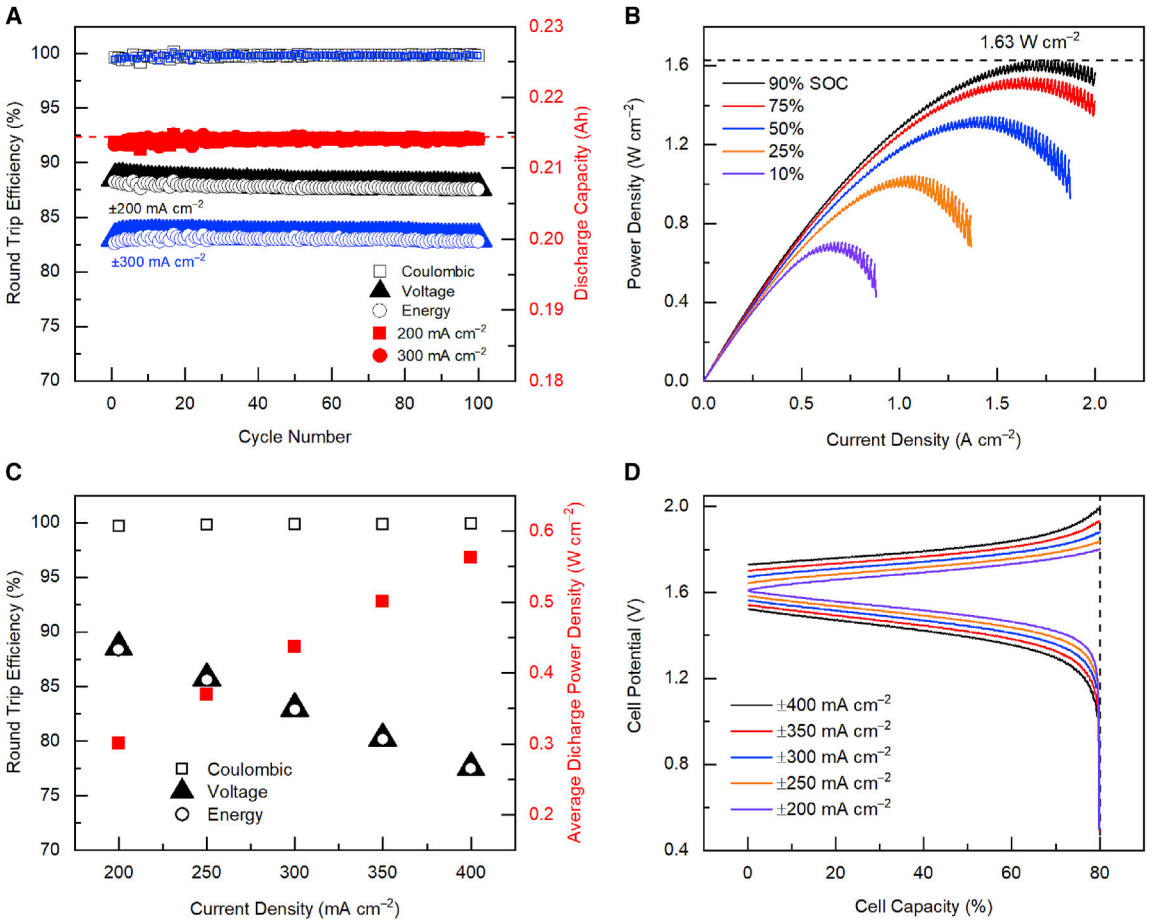

Figure 4. Optimized E-610(K) cell cycling data

(A) Discharge capacity and coulombic, voltage, and energy efficiency per cycle for optimized cell 1 at ±200 mA cm^{-2} (black, red square) and optimized cell 2 at ±300 mA cm^{-2} (blue, red circle) utilizing E-610(K), Bi-plating, 40°C heating, and 1.0 M CrPDTA in 0.1 M PDTA versus unbuffered $Fe(CN)_6$.

(B) Discharge power density as a function of current density at select SOC for optimized cell 2. A maximum power density of 1.63 W cm^{-2} is achieved.

(C) Average efficiencies and discharge power density for optimized cell 2 over 3 cycles at select current densities.

(D) Cell potential during 80% capacity cycling at select current densities for optimized cell 2.

operated for 100 cycles at ±300 mA cm^{-2} with constant VE and exhibited an average CE of 99.7%, an average VE of 83.2%, and an average discharge power density of 433 mW cm^{-2} (Figures 4A and S15A). Linear current sweeps at 500 mA s^{-1} were performed at 10%, 25%, 50%, 75%, and 90% SOC, and a peak discharge power density of 1.63 W cm^{-2} was observed, which more than triples the initial CrPDTA|$Fe(CN)_6$ RFB with Nafion 212 reported value of 0.515 W cm^{-2} and is the highest ever reported for an RFB using K^+ transport (Figures 4B and S15B).[20] To explore where 80% EE cycling could be achieved, cycling at different current densities was then performed, with 3 cycles each at ±200, 250, 300, 350, and 400 mA cm^{-2} to 80% CrPDTA capacity (Figures 4C, 4D, and S15C; Table S3). Greater than 80% EE is achieved with current densities up to ±350 mA cm^{-2} at average discharge power densities up to 0.5 W cm^{-2}, which more than doubles the previous record for RFBs using K^+ transport and is the third highest value for any RFB.[13,27,30] The ±400 mA cm^{-2} cycling demonstrates an average CE of 99.9%, indicating that no appreciable HER increase occurs, and an average discharge power density of 0.562 W cm^{-2}, which is greater than the initially reported CrPDTA|$Fe(CN)_6$ RFB peak power density of 0.515 W cm^{-2}.[20]

This high-power demonstration is significant in illustrating the potential of K^+-based membrane transport paired with high-voltage RFB chemistry. More importantly, these high-performance results were achieved with electrolytes composed of low-cost and scalable materials, with iron and chromium being the top two highest global productions among transition metals and with the chelating agents and ligands already mass produced on an industrial scale.[8,50] System costs are minimized not only by the high-power performance enabled by high operating voltage, which decreases stack size, but by operating in non-corrosive, near-neutral pH. These benign conditions can permit further cost savings from low-cost carbon electrodes and bipolar plates, and an inexpensive, robust bismuth electrocatalyst, while eliminating the need for expensive PFSA membranes. Performance milestones that took VRFBs decades to reach have been achieved within a few years with our CrPDTA chemistry.

Through a systematic investigation of RFB resistances, we report how to decrease and maintain constant ASR through several key cell component considerations. We then demonstrated how these improvements can enable high performance K^+-based CrPDTA|$Fe(CN)_6$ RFBs utilizing highly conductive E-600(K) membranes. A CrPDTA|$Fe(CN)_6$ RFB with Bi-plated electrodes was cycled 200 times with constant VE, the longest yet reported for the system, suggesting that the deposited bismuth remains present in the highly reducing, neutral pH operating conditions. Further, using the discussed ASR minimization techniques, an optimized CrPDTA|$Fe(CN)_6$ RFB utilizing an E-610(K) CEM with Bi-plated electrodes and 40°C cell heating operated with a constant 0.46 Ω-cm^2 ASR, proving that low ASRs can be achieved in non-acidic systems.

Because RFB power performance scales quadratically with voltage (V^2/R), the approach to lower the cell ASR paired with the high cell potential of the CrPDTA|$Fe(CN)_6$ system allowed optimized cells to achieve a maximum discharge power density of 1.63 W cm^{-2} and an average discharge power density of 0.5 W cm^{-2} at 80% round-trip EE, which are the highest values demonstrated for any K^+-based RFB and are higher than all but a few optimized H^+-based VRFBs.[13] Furthermore, the optimized E-610(K) CrPDTA|$Fe(CN)_6$ RFB demonstrated constant VE over 100 cycles at both $\pm$200 and $\pm$300 mA cm^{-2} with average CE above 99.7%, indicating the ASR improvements did not promote increased HER. Further, the inexpensive, non-PFSA E-600(K) membranes showed no long-term degradation, decrease in K^+ conductivity, or active material crossover, demonstrating their robust nature in the RFB conditions, supporting their use for low-cost, large-scale operation. As R_Ω is still the majority of the ASR, further system improvement can be achieved through tailored K^+ membrane design optimizations and other systematic optimizations of the RFB to minimize ASR through minimizing R_Ω, R_{ct}, or R_{mt}. This power-cycling performance represents an important performance milestone for emerging flow battery electrolyte materials, demonstrating a system that can be low cost and high performance without tradeoff.

EXPERIMENTAL PROCEDURES

Resource availability

Lead contact

Further information and requests for resources and reagents should be directed to and will be fulfilled by the lead contact, Michael P. Marshak (Michael.marshak@colorado.edu).

Materials availability

This study did not generate new unique materials.

Data and code availability

Full data are available upon request from the authors.

Electrolyte preparation

All materials were used as received without further purification. Bismuth chloride oxide (98%) and potassium bromide (99% min) were purchased from Alfa Aesar. Potassium tetraborate tetrahydrate (99%, extra pure) was purchased from Acros Organics. Boric acid (ACS reagent) was purchased from Chem-Impex. Potassium ferricyanide (ACS grade) was purchased from LabChem. Potassium ferrocyanide trihydrate (≥99%) was purchased from Fluka. Chromium(III) potassium sulfate dodecahydrate (reagent grade) was purchased from Fisher Science Education. Potassium hydroxide pellets (certified ACS) were purchased from Fisher Chemical. PDTA (≥99.0%) was purchased from Aldrich.

KCrPDTA synthesis was prepared as previously reported.[19] The material was confirmed via UV-visible (UV-vis) peaks at 506 and 382 nm.[20,51] The 1 M KCrPDTA with 0.2 M $B(OH)_3$/0.05 M $K_2B_4O_7$ anolytes used in this work were made by dissolving KCrPDTA (4.474 g, 10 mmol), $B(OH)_3$ (0.124 g, 2 mmol), and $K_2B_4O_7$ (0.153 g, 0.5 mmol) solids in DI H_2O in a 10 mL volumetric flask. The 1 M KCrPDTA with 0.1 M PDTA buffer anolytes used in this work were made in a 10 mL volumetric flask by dissolving KCrPDTA (4.474 g, 10 mmol) to a final solution volume of 10 mL using 5 mL 0.2 M PDTA solution and the remaining deionized (DI) H_2O. The 0.2 M PDTA solutions were made by adding H_4PDTA (6.125 g, 20 mmol) in DI H_2O (80 mL). Then, 5 M KOH was added to adjust the pH to 8.5. The PDTA solution was transferred to a 100 mL volumetric flask, and the volume was adjusted to the line with DI H_2O.

Flow cell measurements

All RFB cycling and power data experiments were performed on an Arbin LBT21084HC workstation galvanostat. All EIS measurements and bismuth plating experiments were conducted on a Gamry Interface 5000 potentiostat/galvanostat. Flow cell components and construction have been reported previously, utilizing a 5 cm^2 single-cell flow battery from Fuel Cell Technologies with Poco graphite blocks and single serpentine flow fields.[20,35,38] Deviations from these reported procedures are listed below. Electrolytes and plating solutions were pumped through the cell with Norprene tubing (3.1 mm ID) and a two-channel peristaltic pump (Cole-Parmer) operating at 60 RPM (resulted in 69 mL min^{-1}). All electrolytes were contained in a 60 mL PFA column component vessel capped with a 58 mm transfer closure with two $^1/_8$″ OD compression fitting ports (Savillex).

Bismuth electrode plating was conducted as previously reported but with step times that were twice as long to account for twice as many carbon papers being utilized in this setup.[19] All flow cell measurements were conducted at room temperature unless otherwise noted. Elevated temperature cells utilized an Omega T-type thermocouple probe and AC cell heaters, both of which were inserted into the aluminum endplates of the RFB and were controlled by an Omega CS8DPT universal digital PID controller.

Flow cell material preparation and assembly

All membranes (3.3 × 3.3 cm) were pre-treated by soaking in DI water for at least 7 days. Two stacked sheets (280 μm thick, 5 cm^2 each) of GDL 39 AA carbon paper (SGL) were heated at 150°C for at least 24 h, to improve electrode wettability, and used on each side with a 1/64″ Viton gasket provided ca. 25% electrode

compression. The cells were bolted together and tightened with a torque wrench set to 5.7 N m. All electrolytes for CrPDTA|$Fe(CN)_6$ RFBs examined in this work were composed of 10 mL aqueous solution of 1 M KCrPDTA as the anolyte and 25 mL aqueous solution of 0.5 M $K_4Fe(CN)_6$/0.1 M $K_3Fe(CN)_6$ as the catholyte (25% molar excess of the Fe(II) species). Because the charged anolyte reduces oxygen, both electrolytes were degassed with nitrogen or argon gas for at least 15 min prior to battery operation.[36,39] Further detailed electrochemical and experimental methods can be found in the supplemental experimental procedures.

SUPPLEMENTAL INFORMATION

Supplemental information can be found online at https://doi.org/10.1016/j.xcrp.2022.101118.

ACKNOWLEDGMENTS

The information, data, or work presented herein was funded by the Advanced Research Projects Agency-Energy (ARPA-E, US Department of Energy) under award number DE-AR0000994 and by the DOE Office of Electricity Energy Storage Program at Pacific Northwest National Laboratory through subcontract 608616. This material is based upon work supported by the National Science Foundation Graduate Research Fellowship Program under grant no. DGE 1650115. Any opinions, findings, and conclusions or recommendations expressed in this material are those of the authors and do not necessarily reflect the views of the National Science Foundation. S.E.W. is funded partially by the King Fellowship from CU Boulder.

AUTHOR CONTRIBUTIONS

B.H.R. synthesized electrolyte formulations and performed all electrochemical experiments in the manuscript. S.E.W. provided insight on electrolyte preparation and collected viscosity data. J.D.S. provided insight on membrane use and preparation. M.P.M. conceived and supervised this project. The manuscript was written through contributions of all authors. All authors have given approval to the final version of the manuscript.

DECLARATION OF INTERESTS

The University of Colorado has filed a PCT patent on some of the flow battery chemistry disclosed in this manuscript. M.P.M. is the founder of a startup company, Otoro Energy, which aims to commercialize some of the battery technology reported in this manuscript. B.H.R.'s current affiliation is Otoro Energy (Boulder, CO, USA).

Received: June 23, 2022
Revised: September 6, 2022
Accepted: October 4, 2022
Published: October 25, 2022

REFERENCES

1. Yang, Z., Zhang, J., Kintner-Meyer, M.C.W., Lu, X., Choi, D., Lemmon, J.P., and Liu, J. (2011). Electrochemical energy storage for green grid. Chem. Rev. *111*, 3577–3613. https://doi.org/10.1021/cr100290v.

2. Soloveichik, G.L. (2015). Flow batteries: current status and trends. Chem. Rev. *115*, 11533–11558. https://doi.org/10.1021/cr500720t.

3. Weber, A.Z., Mench, M.M., Meyers, J.P., Ross, P.N., Gostick, J.T., and Liu, Q. (2011). Redox flow batteries: a review. J. Appl. Electrochem. *41*, 1137–1164. https://doi.org/10.1007/s10800-011-0348-2.

4. Skyllas-Kazacos, M., Chakrabarti, M.H., Hajimolana, S.A., Mjalli, F.S., and Saleem, M. (2011). Progress in flow battery Research and development. J. Electrochem. Soc. *158*, R55–R79. https://doi.org/10.1149/1.3599565.

5. Wang, W., Luo, Q., Li, B., Wei, X., Li, L., and Yang, Z. (2013). Recent progress in redox flow battery Research and development. Adv. Funct. Mater. *23*, 970–986. https://doi.org/10.1002/adfm.201200694.

6. Ponce de León, C., Frías-Ferrer, A., González-García, J., Szánto, D., and Walsh, F.C. (2006). Redox flow cells for energy conversion. J. Power Sources *160*, 716–732. https://doi.org/10.1016/j.jpowsour.2006.02.095.

7. Zeng, Y.K., Zhao, T.S., An, L., Zhou, X.L., and Wei, L. (2015). A comparative study of all-vanadium and iron-chromium redox flow batteries for large-scale energy storage. J. Power Sources *300*, 438–443. https://doi.org/10.1016/j.jpowsour.2015.09.100.

8. Vesborg, P.C.K., and Jaramillo, T.F. (2012). Addressing the terawatt challenge: scalability in the supply of chemical elements for renewable energy. RSC Adv. *2*, 7933–7947. https://doi.org/10.1039/C2RA20839C.

9. Chalamala, B.R., Soundappan, T., Fisher, G.R., Anstey, M.R., Viswanathan, V.V., and Perry, M.L. (2014). Redox flow batteries: an engineering perspective. Proc. IEEE *102*, 976–999. https://doi.org/10.1109/JPROC.2014.2320317.

10. Skyllas-Kazacos, M., Rychcik, M., Robins, R.G., Fane, A.G., and Green, M.A. (1986). New all-vanadium redox flow cell. J. Electrochem. Soc. *133*, 1057–1058. https://doi.org/10.1149/1.2108706.

11. Aaron, D.S., Liu, Q., Tang, Z., Grim, G.M., Papandrew, A.B., Turhan, A., Zawodzinski, T.A., and Mench, M.M. (2012). Dramatic performance gains in vanadium redox flow batteries through modified cell architecture. J. Power Sources *206*, 450–453. https://doi.org/10.1016/j.jpowsour.2011.12.026.

12. Perry, M.L., Darling, R.M., and Zaffou, R. (2013). High power density redox flow battery cells. ECS Trans. *53*, 7–16. https://doi.org/10.1149/05307.0007ecst.

13. Jiang, H.R., Sun, J., Wei, L., Wu, M.C., Shyy, W., and Zhao, T.S. (2020). A high power density and long cycle life vanadium redox flow battery. Energy Storage Mater. *24*, 529–540. https://doi.org/10.1016/j.ensm.2019.07.005.

14. Thurston, J.R., Waters, S.E., Robb, B.H., and Marshak, M.P. (2021). Organic and metal-organic RFBs. In Encyclopedia of Energy Storage, L.F. Cabeza, ed. (Elsevier), pp. 423–435.

15. Waters, S.E., Thurston, J.R., Armstrong, R.W., Robb, B.H., Marshak, M.P., and Reber, D. (2022). Holistic design principles for flow batteries: cation dependent membrane resistance and active species solubility. J. Power Sources *520*, 230877. https://doi.org/10.1016/j.jpowsour.2021.230877.

16. Dmello, R., Milshtein, J.D., Brushett, F.R., and Smith, K.C. (2016). Cost-driven materials selection criteria for redox flow battery electrolytes. J. Power Sources *330*, 261–272. https://doi.org/10.1016/j.jpowsour.2016.08.129.

17. Darling, R.M., Gallagher, K.G., Kowalski, J.A., Ha, S., and Brushett, F.R. (2014). Pathways to low-cost electrochemical energy storage: a comparison of aqueous and nonaqueous flow batteries. Energy Environ. Sci. *7*, 3459–3477. https://doi.org/10.1039/C4EE02158D.

18. Kwabi, D.G., Lin, K., Ji, Y., Kerr, E.F., Goulet, M.-A., De Porcellinis, D., Tabor, D.P., Pollack, D.A., Aspuru-Guzik, A., Gordon, R.G., and Aziz, M.J. (2018). Alkaline quinone flow battery with long lifetime at pH 12. Joule *2*, 1894–1906. https://doi.org/10.1016/j.joule.2018.07.005.

19. Proctor, A.D., Robb, B.H., Saraidaridis, J.D., and Marshak, M.P. (2022). Bismuth electrocatalyst enabling reversible redox kinetics of a chelated chromium flow battery anolyte. J. Electrochem. Soc. *169*, 030506. https://doi.org/10.1149/1945-7111/ac56d3.

20. Robb, B.H., Farrell, J.M., and Marshak, M.P. (2019). Chelated chromium electrolyte enabling high-voltage aqueous flow batteries. Joule *3*, 2503–2512. https://doi.org/10.1016/j.joule.2019.07.002.

21. Huskinson, B., Marshak, M.P., Suh, C., Er, S., Gerhardt, M.R., Galvin, C.J., Chen, X., Aspuru-Guzik, A., Gordon, R.G., and Aziz, M.J. (2014). A metal-free organic–inorganic aqueous flow battery. Nature *505*, 195–198. https://doi.org/10.1038/nature12909.

22. Gahn, R.F., Hagedorn, N.H., and Johnson, J.A. (1985). Cycling performance of the iron-chromium redox energy storage system. In 20th Intersociety Energy Conversion Engineering Conference.

23. Zeng, Y.K., Zhao, T.S., Zhou, X.L., Zeng, L., and Wei, L. (2016). The effects of design parameters on the charge-discharge performance of iron-chromium redox flow batteries. Appl. Energy *182*, 204–209. https://doi.org/10.1016/j.apenergy.2016.08.135.

24. Zeng, Y.K., Zhou, X.L., Zeng, L., Yan, X.H., and Zhao, T.S. (2016). Performance enhancement of iron-chromium redox flow batteries by employing interdigitated flow fields. J. Power Sources *327*, 258–264. https://doi.org/10.1016/j.jpowsour.2016.07.066.

25. Zeng, Y.K., Zhou, X.L., An, L., Wei, L., and Zhao, T.S. (2016). A high-performance flow-field structured iron-chromium redox flow battery. J. Power Sources *324*, 738–744. https://doi.org/10.1016/j.jpowsour.2016.05.138.

26. Yang, Z., Gerhardt, M.R., Fortin, M., Shovlin, C., Weber, A.Z., Perry, M.L., Darling, R.M., and Saraidaridis, J.D. (2021). Polysulfide-permanganate flow battery using abundant active materials. J. Electrochem. Soc. *168*, 070516. https://doi.org/10.1149/1945-7111/ac1036.

27. Lin, K., Chen, Q., Gerhardt, M.R., Tong, L., Kim, S.B., Eisenach, L., Valle, A.W., Hardee, D., Gordon, R.G., Aziz, M.J., and Marshak, M.P. (2015). Alkaline quinone flow battery. Science *349*, 1529–1532. https://doi.org/10.1126/science.aab3033.

28. Liu, T., Wei, X., Nie, Z., Sprenkle, V., and Wang, W. (2016). A total organic aqueous redox flow battery employing a low cost and sustainable methyl viologen anolyte and 4-HO-TEMPO catholyte. Adv. Energy Mater. *6*, 1501449. https://doi.org/10.1002/aenm.201501449.

29. Qian, P., Zhang, H., Chen, J., Wen, Y., Luo, Q., Liu, Z., You, D., and Yi, B. (2008). A novel electrode-bipolar plate assembly for vanadium redox flow battery applications. J. Power Sources *175*, 613–620. https://doi.org/10.1016/j.jpowsour.2007.09.006.

30. Zhou, X.L., Zeng, Y.K., Zhu, X.B., Wei, L., and Zhao, T.S. (2016). A high-performance dual-scale porous electrode for vanadium redox flow batteries. J. Power Sources *325*, 329–336. https://doi.org/10.1016/j.jpowsour.2016.06.048.

31. Zhou, H., Zhang, H., Zhao, P., and Yi, B. (2006). A comparative study of carbon felt and activated carbon based electrodes for sodium polysulfide/bromine redox flow battery. Electrochim. Acta *51*, 6304–6312. https://doi.org/10.1016/j.electacta.2006.03.106.

32. Gao, M., Salla, M., Song, Y., and Wang, Q. (2022). High-power near-neutral aqueous all organic redox flow battery enabled with a pair of anionic redox species. Angew. Chem. Int. Ed. Engl. *61*, e202208223. https://doi.org/10.1002/anie.202208223.

33. Wang, X., Gao, M., Lee, Y.M., Salla, M., Zhang, F., Huang, S., and Wang, Q. (2022). E-blood: high power aqueous redox flow cell for concurrent powering and cooling of electronic devices. Nano Energy *93*, 106864. https://doi.org/10.1016/j.nanoen.2021.106864.

34. Perry, M.L., Rodby, K.E., and Brushett, F.R. (2022). Untapped potential: the need and opportunity for high-voltage aqueous redox flow batteries. ACS Energy Lett. *7*, 659–667. https://doi.org/10.1021/acsenergylett.1c02225.

35. Robb, B.H., Waters, S.E., and Marshak, M.P. (2020). Evaluating aqueous flow battery electrolytes: a coordinated approach. Dalton Trans. *49*, 16047–16053. https://doi.org/10.1039/D0DT02462G.

36. Waters, S.E., Robb, B.H., Scappaticci, S.J., Saraidaridis, J.D., and Marshak, M.P. (2022). Isolation and characterization of a highly reducing aqueous chromium(II) complex. Inorg. Chem. *61*, 8752–8759. https://doi.org/10.1021/acs.inorgchem.2c00699.

37. Ogino, H., Nagata, T., and Ogino, K. (1989). Redox potentials and related thermodynamic parameters of (diaminopolycarboxylato) metal(III/II) redox couples. Inorg. Chem. *28*, 3656–3659. https://doi.org/10.1021/ic00318a009.

38. Reber, D., Thurston, J.R., Becker, M., Pach, G.F., Wagoner, M.E., Robb, B.H., Waters, S.E., and Marshak, M.P. (2022). Mediating anion-cation interactions to improve aqueous flow battery electrolytes. Appl. Mater. Today *28*, 101512. https://doi.org/10.1016/j.apmt.2022.101512.

39. Robb, B.H., Waters, S.E., and Marshak, M.P. (2020). Minimizing oxygen permeation in metal-chelate flow batteries. ECS Trans. *97*, 237–245. https://doi.org/10.1149/09707.0237ecst.

40. Noh, C., Shin, M., and Kwon, Y. (2022). A strategy for lowering cross-contamination of aqueous redox flow batteries using metal-ligand complexes as redox couple. J. Power Sources *520*, 230810. https://doi.org/10.1016/j.jpowsour.2021.230810.

41. Robb, B.H., Waters, S.E., and Marshak, M.P. (2022). High energy density chelated chromium flow battery electrolyte at neutral pH. Chem. Asian J. https://doi.org/10.1002/asia.202200700.

42. Ji, Y., Goulet, M., Pollack, D.A., Kwabi, D.G., Jin, S., Porcellinis, D., Kerr, E.F., Gordon, R.G., and Aziz, M.J. (2019). A phosphonate-functionalized quinone redox flow battery at near-neutral pH with record capacity retention rate. Adv. Energy Mater. *9*, 1900039. https://doi.org/10.1002/aenm.201900039.

43. Jin, S., Fell, E.M., Vina-Lopez, L., Jing, Y., Michalak, P.W., Gordon, R.G., and Aziz, M.J. (2020). Near neutral pH redox flow battery with low permeability and long-lifetime phosphonated viologen active species. Adv. Energy Mater. *10*, 2000100. https://doi.org/10.1002/aenm.202000100.

44. Wang, C., Yu, B., Liu, Y., Wang, H., Zhang, Z., Xie, C., Li, X., Zhang, H., and Jin, Z. (2021). N-alkyl-carboxylate-functionalized anthraquinone for long-cycling aqueous redox flow batteries. Energy Storage Mater. *36*, 417–426. https://doi.org/10.1016/j.ensm.2021.01.019.

45. Saraidaridis, J.D., Darling, R.M., Yang, Z., Shovlin, C., Fortin, M., Robb, B.H., Waters, S.E., and Marshak, M.P. (2022). Transport of ligand coordinated iron and chromium through cation-exchange membranes. J. Electrochem. Soc. *169*, 060532. https://doi.org/10.1149/1945-7111/ac7782.

46. Haynes, W.M. (2012). CRC Handbook of Chemistry and Physics, 93rd Edition (CRC Press).

47. Machado, C.A., Brown, G.O., Yang, R., Hopkins, T.E., Pribyl, J.G., and Epps, T.H. (2021). Redox flow battery membranes: improving battery performance by leveraging structure–property relationships. ACS Energy Lett. *6*, 158–176. https://doi.org/10.1021/acsenergylett.0c02205.

48. Viswanathan, V., Crawford, A., Stephenson, D., Kim, S., Wang, W., Li, B., Coffey, G., Thomsen, E., Graff, G., Balducci, P., et al. (2014). Cost and performance model for redox flow batteries. J. Power Sources *247*, 1040–1051. https://doi.org/10.1016/j.jpowsour.2012.12.023.

49. Li, L., Kim, S., Wang, W., Vijayakumar, M., Nie, Z., Chen, B., Zhang, J., Xia, G., Hu, J., Graff, G., et al. (2011). A stable vanadium redox-flow battery with high energy density for large-scale energy storage. Adv. Energy Mater. *1*, 394–400. https://doi.org/10.1002/aenm.201100008.

50. Darling, R.M. (2022). Techno-economic analyses of several redox flow batteries using levelized cost of energy storage. Curr. Opin. Chem. Eng. *37*, 100855. https://doi.org/10.1016/j.coche.2022.100855.

51. Hecht, M., Schultz, F.A., and Speiser, B. (1996). Ligand structural effects on the electrochemistry of chromium(III) amino carboxylate complexes. Inorg. Chem. *35*, 5555–5563. https://doi.org/10.1021/ic960152o.